

Frankfurt preprint UFTP-436
 Duke preprint DUKE-TH-97-139
 Columbia preprint CU-TP-820

Kaon Interferometry as Signal for the QCD Phase Transition at RHIC [†]

Stefan Bernard ¹, Dirk H. Rischke ², Joachim A. Maruhn ¹, Walter Greiner ¹

¹ Institut für Theoretische Physik der J.W. Goethe-Universität
 Robert-Mayer-Str. 10, D-60054 Frankfurt/M., Germany

² Department of Physics, Duke University
 Durham, NC 27708-0305, U.S.A.

March 1997

Abstract

Pion and kaon correlations in relativistic nuclear collisions are studied in the framework of boost-invariant, cylindrically symmetric hydrodynamics. It is investigated how the inverse widths, R_{out} , R_{side} , of the two-particle correlation functions in out- and side-direction depend on the average transverse momentum K_{\perp} of the particle pair, the initial energy density ϵ_0 , and the equation of state of the system. The QCD transition leads to a time delay in the expansion of the system and consequently to an enhancement of the ratio $R_{\text{out}}/R_{\text{side}}$. This time-delay signal is found to be particularly strong for large average transverse momenta $K_{\perp} \sim 1$ GeV and initial energy densities accessible at RHIC, $\epsilon_0 \sim 10 - 20 \text{ GeV fm}^{-3}$. Neutral kaon pair correlation functions, which are not influenced by final state Coulomb effects and less contaminated by resonance decays than pion correlation functions, seem to be the ideal tool to detect this collective time-delay signature of the QCD transition.

[†]Supported by DFG, BMBF, GSI, and DOE.

1 Introduction

Lattice studies of quantum chromodynamics (QCD) exhibit a chiral symmetry restoring, deconfining transition around a temperature $T_c \sim 160$ MeV (for (net) baryon-free matter) [1]. The only possibility to study this transition and the properties of the high-temperature phase of nuclear matter, the so-called quark–gluon plasma (QGP) [2], under laboratory conditions is via relativistic heavy-ion collision experiments [3].

Promising signals for the detection of the QGP emerge from the influence of the QCD equation of state (EoS) on the collective dynamical evolution of the many-particle system. Such signals have to be studied via relativistic hydrodynamics [4], since that is the only dynamical model which provides a direct link between collective motion and the EoS of strongly interacting matter. For instance, it was shown in [5, 6, 7] that the QCD transition softens the EoS in the transition region and therefore reduces the tendency of matter to expand. This has two important consequences. On one hand, the expansion of the system is delayed and its lifetime is considerably prolonged [5, 6, 7]. On the other hand it was shown in [8, 9] that the reduced expansion tendency of matter leads to a reduction of the transverse directed flow in semi-peripheral heavy-ion collisions.

In [10] the hydrodynamic flow pattern was studied for spherically symmetric (so-called “fireball”) expansion as well as for cylindrically symmetric transverse expansion with longitudinally boost-invariant initial conditions (so-called “Bjorken cylinder” expansion), both as a function of the initial energy density ϵ_0 and a possible finite width ΔT of the QCD transition region. The QCD transition was shown to considerably prolong the lifetime of the expanding system as compared to the expansion of an (ultrarelativistic) ideal gas, provided the initial energy density lies in a certain range of values. This range corresponds to AGS initial energy densities for the fireball geometry, and RHIC initial energy densities for the Bjorken cylinder geometry (for realistic values of the initial thermalization time scale τ_0). Motivated by Pratt’s and Bertsch’s conjecture [11, 12], it was shown in [10], that for both geometries the prolongation of the lifetime could be experimentally observable via the ratio $R_{\text{out}}/R_{\text{side}}$ of the inverse widths of the two-particle correlation functions in out- and side-direction, since this ratio follows the behaviour of the lifetimes rather closely.

In this paper we extend the investigations of [10] for the Bjorken cylinder geometry in two ways. First, we study two-kaon in addition to two-pion interferometry. While pion correlation functions are contaminated to a large extent by resonance decays, one expects these to be of minor influence in the case of kaons [13]. In addition, neutral kaon correlation functions are, in contrast to the pionic ones, not distorted by final state Coulomb effects which introduce an additional uncertainty in experimental data.

Second, we now present a systematic study of R_{out} , R_{side} , and their ratio as a function of initial energy density ϵ_0 and of the mean transverse pair momentum K_{\perp} at midrapidity. As in [10], we take an EoS with a first order phase transition ($\Delta T = 0$) as well as an EoS with a finite width $\Delta T = 0.1 T_c$ (as an upper limit deduced from QCD lattice calculations [1]), and compare the enhancement of $R_{\text{out}}/R_{\text{side}}$ relative to the ideal gas case.

We find that the excitation function of $R_{\text{out}}/R_{\text{side}}$ for kaons again mirrors closely that of the lifetime of the system, and has a maximum around the same initial energy density ϵ_0

as for pions. Due to kinematical reasons the ratio is, however, somewhat smaller for kaons with small average transverse pair momentum $K_{\perp} < m_K = 497$ MeV as compared to the pion case. On the other hand, for high $K_{\perp} \sim 1$ GeV, it is nearly of the same order as that for pions.

We also study separately the dependence of R_{out} and R_{side} on ϵ_0 and K_{\perp} . As expected, these quantities in general decrease with increasing K_{\perp} at fixed ϵ_0 . An important exception is the situation around values of $\epsilon_0 \sim 10 - 20$ GeV fm⁻³, where the time-delay signal is most pronounced. For these initial energy densities and in the case of a first order transition, $\Delta T = 0$, we find that R_{out} actually increases as a function of K_{\perp} , both for pions and kaons. We analyze this behaviour in detail studying the emission function and its variances [14].

The outline of the paper is as follows. In Section 2 we briefly discuss the hydrodynamic model, the EoS used, and the basic formulae to derive single inclusive particle spectra and two-particle correlation functions from the hydrodynamic solution. In Section 3 we present our results. A summary and conclusions are given in Section 4. An appendix contains technical details on the calculation of the variances of the emission function. Natural units $\hbar = c = k_B = 1$ are used throughout this work.

2 Hydrodynamics and Particle Spectra

2.1 The hydrodynamic model

Hydrodynamics is equivalent to local conservation of energy and momentum,

$$\partial_{\mu} T^{\mu\nu} = 0 , \tag{1}$$

plus additional conservation equations for the (net) 4-current of any conserved charge in the system. The latter will not be considered here, since our focus of interest, the central (rapidity) region of ultrarelativistic heavy-ion collisions, is expected to be essentially free of (net) charges due to the limited nuclear stopping power.

In order to solve the relativistic hydrodynamic equations (1) we make the assumption of local thermodynamic equilibrium, the so-called “ideal fluid approximation”. This approximation, although commonly employed throughout the literature, is rather restrictive, since the fluid is certainly out of thermodynamic equilibrium in the early and late stages of a heavy-ion collision. On the other hand, a commonly accepted, causal theory of dissipative relativistic hydrodynamics, which would account for non-equilibrium phenomena, does not yet exist [4]. For the moment we have to rely on the assumption that (local) thermalization does indeed occur after the initial pre-equilibrium stage which is dominated by (hard) parton-parton scattering processes (for collisions at RHIC energies). Arguments in favour of this assumption are made in [15]. We then describe the system’s evolution from this point on via ideal fluid-dynamics, until dissipative effects in the final stages prior to decoupling become large and the assumption of local thermodynamical equilibrium again breaks down.

In the ideal fluid approximation, the energy-momentum tensor reads [16]

$$T^{\mu\nu} = (\epsilon + p) u^{\mu} u^{\nu} - p g^{\mu\nu} . \tag{2}$$

Here, ϵ , p are energy density and pressure in the rest frame of the fluid, while $u^\mu = \gamma(1, \boldsymbol{\beta})$ and $g^{\mu\nu} = \text{diag}(+, -, -, -)$ are the 4-velocity of the fluid and the metric tensor, respectively ($\boldsymbol{\beta}$ is the 3-velocity, $\gamma \equiv (1 - \boldsymbol{\beta}^2)^{-1/2}$ is the gamma factor).

Our model for the dynamics of central ultrarelativistic heavy-ion collisions is the so-called ‘‘Bjorken cylinder’’ expansion [17], i.e., it assumes cylindrical symmetry perpendicular to the beam axis (taken to be the z -axis throughout this work) and a scaling solution for the longitudinal expansion ($\beta^z = z/t$). Note that due to the details of the mini-jet production mechanism, these assumptions about the symmetries of the system are not valid per single event [18]. On the other hand, they seem quite reasonable on an event-average basis.

A consequence of longitudinal scaling is boost-invariance along the beam axis. It is therefore sufficient to solve the system of four hydrodynamic equations (1) at $z = 0$, where it reduces to

$$\partial_t E + \partial_r [(E + p)\beta] = - \left(\frac{\beta}{r} + \frac{1}{t} \right) (E + p) , \quad (3)$$

$$\partial_t M + \partial_r (M\beta + p) = - \left(\frac{\beta}{r} + \frac{1}{t} \right) M . \quad (4)$$

Here, β is the radial component of the transverse velocity, and we used the definitions $E \equiv T^{00}$, $M \equiv T^{0r}$ (r as index for the radial component of the energy-momentum tensor). In order to solve the (effectively (1+1)-dimensional) system (3,4), we apply the same scheme used in [10], i.e., we employ Sod’s operator splitting method [19] to account for the source terms on the right-hand side, and the numerically well-tested relativistic HLLE algorithm [6, 20] for the one-dimensional hydrodynamic transport on the left-hand side of (3,4). The HLLE scheme was shown to yield excellent results in particular for equations of state with phase transitions [6, 21].

2.2 The equation of state

As mentioned in the introduction, the advantage of hydrodynamics to model the dynamics of relativistic heavy-ion collisions is that this is the only approach which directly relates observable collective flow phenomena to the EoS of hot and dense nuclear matter. Formally, specifying an EoS closes the coupled system of hydrodynamic equations. In the particular case of vanishing conserved (net) charges considered here, the system (3,4) is closed by an EoS of the form $p(\epsilon)$. In the ideal fluid approximation the emerging flow pattern is completely determined by the choice of this EoS and the initial conditions.

In the present work we study hydrodynamic expansion for three different equations of state. The simplest one is the EoS of an ultrarelativistic ideal gas,

$$p(\epsilon) = c_s^2 \epsilon , \quad (5)$$

where $c_s = 1/\sqrt{3}$ is the velocity of sound. This is commonly taken to be a reasonable first approximation for a hadronic matter EoS in the central region of an ultrarelativistic heavy-ion collision, since here the system is hot, $T > m_\pi$, and thus dominated by pions, which are

the lightest hadrons. The EoS (5) has a constant pressure gradient $dp/d\epsilon \equiv c_s^2 = 1/3$ for all energy densities.

To study the effects of a (phase) transition to QGP on the dynamics of the system, we use the following parametrization of the entropy density as function of temperature [7, 10, 22],

$$\frac{s}{s_c}(T) = \left[\frac{T}{T_c} \right]^3 \left(1 + \frac{d_Q - d_H}{d_Q + d_H} \tanh \left[\frac{T - T_c}{\Delta T} \right] \right). \quad (6)$$

Here, $s_c = (d_Q + d_H)\pi^2 T_c^3/45$ is the entropy density at the critical temperature T_c , and d_Q and d_H are the number of (massless) degrees of freedom in the QGP and the hadronic phase, respectively (we fix $d_Q = 37$ and $d_H = 3$ throughout this work, for the effect of other choices on the dynamics of the system, see [10]). The function $p(\epsilon)$ then follows from thermodynamical relations and is used in the hydrodynamic model in tabular form. Eq. (6) accounts for a possible finite width ΔT of the transition. Present QCD lattice data [1] indicate $0 \leq \Delta T < 0.1 T_c$.

In the limit $\Delta T = 0$, eq. (6) exhibits a first order phase transition between an ultrarelativistic gas of hadrons described by the EoS (5), and a (net) baryon-free QGP consisting of gluons and u and d quarks (and antiquarks) described by the well-known MIT bag EoS [23]. Energy density and pressure in the QGP phase are then $\epsilon_q = d_Q \pi^2 T^4/30 + B$, $p_q = (\epsilon_q - 4B)/3$, while the corresponding quantities in the hadronic phase are $\epsilon_h = d_H \pi^2 T^4/30$, $p_h = \epsilon_h/3$. $B = \frac{1}{2} [(d_Q - d_H)/(d_Q + d_H)] T_c s_c$ is the MIT bag constant, if one measures energy densities in units of the critical enthalpy density $w_c \equiv \epsilon_c + p_c = T_c s_c$ (p_c is the pressure at T_c ; for our choice $d_Q/d_H = 37/3$ and $T_c = 160$ MeV, $T_c s_c \simeq 0.75$ GeV fm⁻³ in physical units). Besides this first order transition with $\Delta T = 0$, we also consider a transition with a finite width $\Delta T = 0.1 T_c$ to cover present uncertainties in the QCD EoS. Note, however, that a finite width would also naturally emerge in any finite system, even if the transition is of first order in the thermodynamic limit [24].

The three different equations of state are displayed in Fig. 1. Part (a) shows the entropy density divided by T^3 and (b) the energy density divided by T^4 as functions of temperature. For the equations of state with a transition, at $T = T_c$ both quantities exhibit the strong increase (or even a discontinuity) observed in lattice calculations. Part (c) shows the pressure and (d) the velocity of sound squared, $c_s^2 \equiv dp/d\epsilon$, as functions of energy density. While for the ideal gas EoS (dashed lines) $c_s^2 = 1/3$ is constant for all energy densities, this is different for the EoS with a first order phase transition, $\Delta T = 0$ (full lines), and the EoS with a transition of finite width $\Delta T = 0.1 T_c$ (dotted lines). The pressure gradient $c_s^2 = dp/d\epsilon$ vanishes for $\Delta T = 0$ as long as matter is in the mixed phase, $\epsilon_H \equiv \epsilon_h(T_c) < \epsilon < \epsilon_Q(T_c) \equiv \epsilon_q$. For parts of the system, which pass through the corresponding region of energy densities, the tendency to expand is then considerably reduced compared to the ideal gas case, which results in a prolonged lifetime of the system [6, 7, 10, 11]. For the transition with finite width $\Delta T = 0.1 T_c$, the pressure gradients are finite, but nevertheless smaller than for the ideal gas. Thus, again the system's lifetime will be prolonged [7, 10].

2.3 Particle spectra and interferometry

In a heavy-ion collision, the ideal fluid approximation breaks down in parts of the system which become so dilute that the collision rates between the particles are smaller than the (local) expansion rate of the system and thus local thermodynamic equilibrium can no longer be maintained. These parts of the system decouple (“freeze out”) from the hydrodynamic evolution and, eventually, the corresponding particles freely stream to the detectors. In a rigorous sense, on one hand they can no longer be described in the hydrodynamical framework, while on the other, the energy and momentum carried away by these particles might influence the hydrodynamic evolution of the rest of the system.

Although attempts have been made [25, 26], up to now no commonly accepted, consistent description of this so-called “freeze-out” process exists for the hydrodynamical description of heavy-ion collisions. The common way to treat this problem is to solve the hydrodynamical equations in the whole forward light cone and a posteriori identify those parts of the system as decoupled, which have cooled below a certain freeze-out temperature T_f or whose density has dropped below a freeze-out density n_f . Final particle spectra are then calculated along the freeze-out hypersurface, $\Sigma(x)$, defined by the condition $T(x) = T_f$, or $n(x) = n_f$, respectively.

Here we also follow this prescription and employ the approach of Cooper and Frye [27] to calculate the particle spectra (see e.g. [28] for a (1+1)–dimensional application). In our case of vanishing (net) charges, the particle density is a function of temperature only, and thus freeze-out at constant density is equivalent to freeze-out at constant temperature. The freeze-out temperature is here taken as a free parameter in the range $(0.7-1) T_c \simeq (110-160)$ MeV.

The single inclusive momentum distribution of “frozen-out” particles, i.e., particles whose world lines cross the 3–dimensional hypersurface Σ in 4–dimensional space–time is then given by [27]

$$E \frac{dN}{d^3\mathbf{k}} = \frac{d}{(2\pi)^3} \int_{\Sigma} d\Sigma \cdot k f(k \cdot u/T) . \quad (7)$$

In our case of pions or kaons, $f(z) = (e^z - 1)^{-1}$ is the Bose–Einstein distribution function. $d\Sigma_{\mu}$ is the normal vector on the (local) hypersurface element Σ^{μ} , and the integration runs over the complete freeze-out hypersurface Σ . Note that, while T is per our definition of freeze-out constant along Σ , the fluid velocity u^{μ} is not.

The Cooper–Frye formula (7) is strictly valid only along space-like parts of the hypersurface Σ , i.e., where the normal vector $d\Sigma_{\mu}$ is time-like. For time-like parts of Σ (space-like $d\Sigma_{\mu}$), however, $d\Sigma \cdot k$ can in principle become negative, corresponding to particles which re-enter the fluid and thus do not decouple from the system. From the physical point of view, this “negative” number of particles should not enter the single inclusive spectrum of frozen-out particles on the left-hand side of (7). Therefore, modifications of the Cooper–Frye formula have been proposed [25, 29], which correct for this. They shall, however, not be employed here, because for the hydrodynamic solutions studied in the following we found the collective flow across the freeze-out surface to be rather strong. The maximum of the single–particle distribution function f is therefore shifted in a way which renders the number of particles with given 4–momentum k^{μ} that actually re-enter the fluid negligible. We shall

quantify this statement below (cf. discussion of Figs. 7, 8).

The two-particle correlation function of two identical particles with momenta $\mathbf{k}_1, \mathbf{k}_2$ is defined as the ratio of the two-particle probability $P(\mathbf{k}_1, \mathbf{k}_2)$ to the product of the single-particle probabilities for uncorrelated particles,

$$C_2(\mathbf{k}_1, \mathbf{k}_2) = \frac{P(\mathbf{k}_1, \mathbf{k}_2)}{P(\mathbf{k}_1)P(\mathbf{k}_2)}. \quad (8)$$

We follow the method outlined in [10, 11, 30, 31] to compute (8). Introducing the average 4-momentum of the particle pair $K^\mu = (k_1^\mu + k_2^\mu)/2$, and the relative 4-momentum $q^\mu = k_1^\mu - k_2^\mu$, and assuming that the particle source is chaotic and sufficiently large, the two-particle correlation function for bosons can be written as [10, 31]

$$C_2(\mathbf{k}_1, \mathbf{k}_2) = 1 + \frac{\left| \frac{d}{(2\pi)^3} \int_{\Sigma} d\Sigma \cdot K \exp[iq \cdot \Sigma] f(K \cdot u/T) \right|^2}{E_1 [dN/d^3\mathbf{k}_1] E_2 [dN/d^3\mathbf{k}_2]}. \quad (9)$$

For the Bjorken cylinder geometry, the number of independent variables can be reduced due to rotational symmetry around the beam axis. As in [10], we focus on the correlation functions of particles emitted at midrapidity ($K^z = q^z = 0$). We choose the coordinate system such that $\mathbf{K} = (K_\perp, 0, 0)$, $\mathbf{q}_{\text{out}} = (q_{\text{out}}, 0, 0)$ for the component of \mathbf{q} parallel to \mathbf{K} , and $\mathbf{q}_{\text{side}} = (0, q_{\text{side}}, 0)$ for the component of \mathbf{q} perpendicular to \mathbf{K} . With these assumptions, $C_2(K, q_{\text{out}}, q_{\text{side}})$ becomes a function of three independent variables only.

The so-called out- and side-correlation functions are now defined as

$$C_{2,\text{out}}(q_{\text{out}}) \equiv C_2(K_\perp, q_{\text{out}}, 0), \quad (10)$$

$$C_{2,\text{side}}(q_{\text{side}}) \equiv C_2(K_\perp, 0, q_{\text{side}}). \quad (11)$$

We then define the inverse width of the correlation functions in out- and side-direction by

$$R_{\text{out}} \equiv \frac{1}{q_{\text{out}}^*}, \quad R_{\text{side}} \equiv \frac{1}{q_{\text{side}}^*}, \quad (12)$$

where q_{out}^* is determined by $C_{2,\text{out}}(q_{\text{out}}^*) = 1.5$, and q_{side}^* analogously. The inverse widths (12) are a qualitative measure for the duration of particle emission and the transverse size of the source. Their quantitative values, however, depend on the initial size of the system, R_0 , on the transverse momentum K_\perp , as well as on the details of the hydrodynamic flow pattern at freeze-out [11, 14, 31]. As argued in [10], these dependences should in principle largely cancel out if one considers the *ratio* of the inverse widths, $R_{\text{out}}/R_{\text{side}}$. In [10] it was also shown that, for the spherical expansion as well as for the Bjorken cylinder expansion, this ratio is a good *qualitative* measure for the lifetime of the system. The explicit form of (9) for the Bjorken cylinder geometry was given in Appendix B of [10] and shall not be repeated here.

For the side-correlation function, the single-particle spectra in the denominator of (9) are equal (because of rotational symmetry, the single-particle spectrum can only depend on the modulus of the transverse momentum, which is equal for the two particles, $\mathbf{k}_1 =$

$(K_\perp, q_{\text{side}}/2, 0)$, $\mathbf{k}_2 = (K_\perp, -q_{\text{side}}/2, 0)$ for pairs at midrapidity), while for the out–correlation function, they are approximately equal as long as the modulus of the relative momentum, q_{out} , of the particle pair is small compared to K_\perp (note that $\mathbf{k}_1 = (K_\perp + q_{\text{out}}/2, 0, 0)$, $\mathbf{k}_2 = (K_\perp - q_{\text{out}}/2, 0, 0)$ for pairs at midrapidity). Furthermore, in this case $K^0 \equiv (k_1^0 + k_2^0)/2 \simeq \sqrt{K_\perp^2 + m^2} \equiv E_K$, and the correlation function can be approximated as [14]

$$C_2(\mathbf{K}, \mathbf{q}) \simeq 1 + \left| \frac{\int d^4x \exp[iq \cdot x] S(x, K)}{\int d^4x S(x, K)} \right|^2 \equiv 1 + |\langle \exp[iq \cdot x] \rangle|^2, \quad (13)$$

where

$$S(x, K) \equiv \frac{d}{(2\pi)^3} \int_\Sigma d\Sigma \cdot K f(K \cdot u/T) \delta^{(4)}(x - \Sigma) \quad (14)$$

is the so-called *emission function* of the source, and the right-hand side of (13) defines the average $\langle \cdot \rangle$. In the following we shall make the Boltzmann approximation for the single–particle distribution function, $f(z) \simeq e^{-z}$, which usually holds to good accuracy, especially for large average pair momenta K_\perp .

In the case that the emission function is Gaussian in space–time, the correlation function can be written in the form (again, we focus on midrapidity pairs, $K^z = q^z = 0$) [14]

$$C_2(K_\perp, q_{\text{out}}, q_{\text{side}}) \simeq 1 + \exp \left[-\hat{R}_{\text{side}}^2 q_{\text{side}}^2 - \hat{R}_{\text{out}}^2 q_{\text{out}}^2 \right], \quad (15)$$

where the (K_\perp –dependent) so-called “side–” and “outwards radii” \hat{R}_{side} , \hat{R}_{out} of the correlation function are related to the variances of the emission function via [14]

$$\hat{R}_{\text{out}}^2 \equiv \langle \tilde{x}^2 \rangle - 2\beta_K \langle \tilde{x}\tilde{t} \rangle + \beta_K^2 \langle \tilde{t}^2 \rangle, \quad (16)$$

$$\hat{R}_{\text{side}}^2 \equiv \langle \tilde{y}^2 \rangle. \quad (17)$$

Here $\beta_K = K_\perp/E_K$ is the (approximate) transverse velocity of the particle pair and $\tilde{x} \equiv x - \langle x \rangle$ (\tilde{t} , \tilde{y} are defined analogously). Note that, in the case of a Gaussian source leading to the correlation function (15), the inverse widths defined in (12) are related to the radii (16,17) via $R_{\text{out,side}} \simeq 1.2 \hat{R}_{\text{out,side}}$. As will be seen in the next section, this formula holds to astonishingly good approximation in the cases considered here, even when the emission functions do not resemble Gaussians. The eqs. (16,17) therefore allow for a reasonable qualitative and quantitative understanding of the shape of the source or the emission function, respectively. The explicit formulae for the variances required to calculate $\hat{R}_{\text{out,side}}$ for the Bjorken cylinder expansion are given in the appendix.

We finally note that other parametrizations of the correlation function, such as the Yano–Koonin–Podgoretskii approach [32], may be more advantageous than the standard (Pratt–Bertsch) parametrization from the point of view of obtaining a better *quantitative* estimate of the variances of the emission function [14]. For studying the *qualitative* behaviour of the proposed time–delay signature, however, the standard parametrization proves to be sufficient.

3 Results

For the Bjorken cylinder expansion one has to specify an initial (proper) time τ_0 for the expansion in order to avoid the divergence at $t = 0$ in eqs. (3,4). Physically, this time corresponds to the thermalization time scale prior to which initial, non-equilibrium parton-parton scattering processes dominate the dynamical evolution. Only for times $\tau \geq \tau_0$, dynamics can be described by means of (ideal) hydrodynamics. According to the “hot-gluon” scenario [15], $\tau_0 \simeq 0.5$ fm for central Au+Au-collisions at RHIC. Since the transverse radius of the hot central zone in such collisions is of the order $R_0 = 5$ fm, we fix $\tau_0 = 0.1 R_0$ in the following. The dependence of the hydrodynamic flow pattern on varying τ_0 as well as the initial energy density ϵ_0 and the EoS was discussed in detail in [10] (cf. Figs. 7-9 therein) and shall not be repeated here.

In particular, it was found in [10] that, for fixed average pion pair momentum $K_\perp = 300$ MeV and for an initial energy density $\epsilon_0 = 18.75 T_c s_c$, in the case of the QCD transition the experimentally measurable ratio $R_{\text{out}}/R_{\text{side}}$ was considerably enhanced over the ideal gas case, reflecting the delay in the expansion of the system due to the softening of the EoS in the transition region. This is once more shown in Fig. 2 (thin lines) for the hydrodynamic expansion with a first order phase transition ($\Delta T = 0$, $d_Q/d_H = 37/3$, $m_\pi = 138$ MeV). The three curves correspond to different freeze-out temperatures $T_f = 0.7 T_c$ (full lines), $T_f = 0.9 T_c$ (dotted lines), and $T_f = T_c$ (dashed lines). In this work we study this *time-delay signature of the QCD transition* not only as a function of ϵ_0 , but also its dependence on K_\perp , both for pions and kaons and for the three different equations of state discussed in Subsection 2.2.

Note that all correlation functions in this work are calculated taking the finite mass of the respective particles into account, but for the fluid evolution, hadron matter is considered to be an ultrarelativistic ideal gas. While this appears inconsistent from a rigorous point of view, quantitatively we do not expect a finite pion mass in the EoS to severely affect the hydrodynamical evolution prior to decoupling, since the freeze-out temperatures considered here are around or even above m_π . Kaons in the hadronic phase are, on the other hand, suppressed by their larger mass, $m_K > T_c$. Therefore, the effect of these particles on the hydrodynamic evolution is expected to be small. This view is supported by the results of [33]. Moreover, small differences in the hydrodynamic evolution tend to have an even smaller impact on the correlation functions (which represent in a certain sense averages over the dynamical evolution) and thus on R_{out} and R_{side} .

The thick lines in Fig. 2 represent our new results for kaons ($m_K = 497$ MeV, $K_\perp = 300$ MeV). For these heavier mesons we also observe a local maximum in the excitation function, which again mirrors closely the prolongation of the lifetime of the system around $\epsilon_0 \simeq 18.75 T_c s_c$. Such a behaviour is *not* seen in the ideal gas case, where $R_{\text{out}}/R_{\text{side}}$ varies rather smoothly (for the sake of clarity, we do not show results for the ideal gas in Fig. 2; for that case see, for instance, Figs. 3, 5 below and Fig. 17 (a) in Ref. [10]). Finally, note that for $K_\perp = 300$ MeV, the enhancement is nearly independent of the freeze-out temperature both for pions as well as for kaons.

For $K_\perp = 300$ MeV the absolute magnitude of $R_{\text{out}}/R_{\text{side}}$ is about a factor of 2 smaller for

kaons than for pions. The reason is the higher mass of the kaons compared to pions which leads, for the comparatively small value of $K_{\perp} = 300$ MeV, to a considerable difference in the velocity of the kaon pair, $\beta_K \simeq 0.52$, as compared to a pion pair with the same K_{\perp} , $\beta_K \simeq 0.91$. In Figs. 7, 8 below we shall explicitly show that the radii (16,17) are reasonably good approximations for the actual inverse widths of the correlation functions. The most important term in (16) turns out to be $\beta_K^2 \langle \tilde{t}^2 \rangle$. Since $\beta_K^2 \simeq 0.27$ for the kaon pair, but $\beta_K^2 \simeq 0.83$ for the pion pair, even if the time variances $\langle \tilde{t}^2 \rangle$ of the emission functions for kaon and pion pairs were roughly equal, the outward radius would turn out to be much smaller in the kaon case.

In fact, the time variance for the kaon emission function is in general smaller than that of the pion source. In order to understand this, note that the maximum of the emission function is typically located near points of the freeze-out hypersurface where the particle pair velocity β_K matches the fluid velocity β , since this minimizes the argument of the exponential term $\exp[-K \cdot u/T]$ in the emission function. For a larger particle mass, however, the emission function decreases faster around this maximum, which in turn reduces its variance as compared to the case of a smaller mass particle. Since this effect, however, also influences the spatial variance of the emission function, we expect it to (roughly) cancel out in the ratio $R_{\text{out}}/R_{\text{side}}$. Thus, the suppression of $R_{\text{out}}/R_{\text{side}}$ for kaons as observed in Fig. 2 is mainly due to the smaller kaon pair velocity.

On the other hand, following this argument we expect that for increasing values of K_{\perp} , for which the pair velocity for kaons is closer to the causal limit (and to that of pions), $R_{\text{out}}/R_{\text{side}}$ should approach similar values as for pions. This is indeed seen to be the case in Fig. 3 where we plot $R_{\text{out}}/R_{\text{side}}$ for $K_{\perp} = 700$ MeV and $\Delta T = 0$. As in the pion case, there is a strong enhancement of about a factor of 2 over the corresponding ideal gas case (thin lines) for all three freeze-out temperatures. On the other hand, the dependence of $R_{\text{out}}/R_{\text{side}}$ on the freeze-out temperature is larger than at $K_{\perp} = 300$ MeV (cf. Fig. 2). The time-delay signal is strongest for late freeze-out ($T_f \sim 0.7 T_c$).

To study the influence of K_{\perp} on the correlation signal in more detail, we present in Fig. 4 the ratio $R_{\text{out}}/R_{\text{side}}$ as a function of K_{\perp} at fixed $\epsilon_0 = 18.75 T_c s_c$, i.e., where the time-delay signal is maximized, and for the case of a first order transition in the EoS. For pions (thin lines) as well as for kaons (thick lines) we observe a strong increase of the ratio with K_{\perp} . While for pions, $R_{\text{out}}/R_{\text{side}}$ is of order 3 already at low momenta, the ratio for kaons increases only gradually from around 1 at $K_{\perp} = 100$ MeV, on account of the above discussed suppression due to the smaller kaon pair velocity. As expected, for high momenta, $K_{\perp} \sim 1$ GeV, $R_{\text{out}}/R_{\text{side}}$ for kaons approaches values comparable to those for pions, since both pion and kaon pair velocities approach unity.

It is also seen from Fig. 4 that the observation made in [10] that the time-delay signal does not depend strongly on the freeze-out temperature is not valid in general and was only due to the specific choice $K_{\perp} = 300$ MeV in that work. The sensitivity of the value of $R_{\text{out}}/R_{\text{side}}$ on the freeze-out temperature increases with K_{\perp} , such that $R_{\text{out}}/R_{\text{side}}$ is the larger the smaller the freeze-out temperature is and may vary up to 20% for freeze-out between $T_f = 0.7 T_c$ and $T_f = T_c$.

In Fig. 5 we present the main result of the present work: shown are surface plots of

$R_{\text{out}}/R_{\text{side}}$ in the $(\epsilon_0 - K_{\perp})$ -plane. The freeze-out temperature was fixed at $T_f = 0.7 T_c$. Fig. 5 (a) shows the ratio of inverse widths for pions and $\Delta T = 0$ (solid lines) versus the ideal gas case (dotted lines). In part (b) the same is shown for $\Delta T = 0.1 T_c$, while (c) and (d) show the corresponding results for kaons. As one observes, the overall behaviour of $R_{\text{out}}/R_{\text{side}}$ is rather similar for pions, Figs. 5 (a,b), as for kaons, parts (c,d). In accordance with Fig. 4 and for the (kinematic) reasons discussed above, the ratio at low K_{\perp} is smaller for kaons than for pions. Also, the enhancement over the ideal gas case is less pronounced in the case of a smooth transition, $\Delta T = 0.1 T_c$, than for a first order phase transition, for reasons discussed in detail in Ref. [10].

The most important property of Fig. 5 is to allow to identify the range of initial energy densities and transverse pair momenta required to maximize the time-delay signature. For our choice of $\tau_0 = 0.1 R_0 \simeq 0.5$ fm, the signal is maximized for initial energy densities around $\epsilon_0 \sim 20 T_c s_c \simeq 15$ GeV fm⁻³. For smaller (larger) τ_0 , the respective values for ϵ_0 increase (decrease), as explained in [10]. These values are well above the soft region of the EoS, cf. Fig. 1 (d). As discussed in detail in Ref. [10], this is due to the strong longitudinal motion in scaling hydrodynamics and opens the possibility to observe the time-delay effect at the RHIC collider. Moreover, Fig. 5 confirms that, for sufficiently high K_{\perp} , the signal is as strong for kaons as for pions. Kaon interferometry is, however, advantageous from the experimental point of view, since kaon yields in general are less contaminated by resonance decays, while neutral kaon correlations in particular are not subject to Coulomb distortions from final state interactions.

In the following, we want to elucidate the behaviour of $R_{\text{out}}/R_{\text{side}}$ in greater detail by studying the inverse widths separately as functions of ϵ_0 and K_{\perp} . Fig. 6 shows (a,c) R_{out} and (b,d) R_{side} both for (a,b) pions and (c,d) kaons for the case of a first order phase transition, $\Delta T = 0$. As one observes, for fixed K_{\perp} , R_{side} increases slowly with ϵ_0 . This behaviour is naturally explained by the fact that higher initial energy densities drive the transverse expansion of the system more strongly (cf. Ref. [10] for the explicit hydrodynamic solutions), which increases the transverse size of the source. On the other hand, for fixed ϵ_0 , R_{side} slowly decreases with increasing K_{\perp} . To understand this quantitatively, recall that the emission function (14) has a maximum where $K \cdot u$ is minimized. For larger pair momenta K_{\perp} (larger pair velocities β_K) the emission function $S(x, K) \sim \exp[-K \cdot u/T]$ will drop faster in the region around the maximum, which in turn makes the source appear smaller.

On the other hand, the ϵ_0 -dependence of R_{out} shows again clearly the time-delay signature of the QCD transition. An unexpected feature is, however, that R_{out} *increases* with K_{\perp} at fixed ϵ_0 , at least for the case $\Delta T = 0$ and for initial energy densities below about $100 T_c s_c$. According to the above argument, R_{out} is expected to decrease as well, and the time-delay signature of Fig. 5 solely due to the fact that the decrease of R_{out} is *slower* than that of R_{side} .

In order to understand why this is not the case for $\Delta T = 0$, let us first consider a situation where this expectation is actually fulfilled. Let us consider the hydrodynamic expansion in the case of a smooth transition $\Delta T = 0.1 T_c$ and for an initial energy density $\epsilon_0 = 18.75 T_c s_c$ (cf. Fig. 9 (c) of Ref. [10]). In Fig. 7 (a) we show the corresponding isotherms in the $(t - r)$ -plane (this figure is identical with Fig. 9 (d) of [10]), part (b) shows the flow velocity β along

the freeze-out hypersurface, i.e., in our case the isotherm with $T = 0.7T_c$ in Fig. 7 (a). Since the mapping of the isotherm on time is unique we prefer to plot β as function of t rather than as function of r , which, considering the shape of the isotherm, is obviously not unique.

In Fig. 7 (c) we show the emission functions $S(x, K)$ for pions, integrated over ϕ and η (i.e., more precisely, the integrand of eq. (29) in the appendix), as a function of time along the freeze-out isotherm for three different values of the average transverse pair momentum, $K_\perp = 300, 700,$ and 1000 MeV. As one expects, for larger pair momenta/velocities the maximum of the emission function shifts to regions of higher transverse velocity on the hypersurface, i.e., to earlier times. Also, in confirmation of the above argument, the emission function becomes narrower, which reflects in a decreasing R_{out}^2 , as shown in Fig. 7 (e). As expected, R_{side}^2 decreases with K_\perp , too, although this cannot be seen directly from the presentation of the emission function in Fig. 7 (c).

Further understanding of this result can be gained by studying the radii (16,17). According to eq. (16), \hat{R}_{out}^2 consists of three different terms. The dashed line in Fig. 7 (e) shows the actual time variance $\langle \tilde{t}^2 \rangle$ of the emission function. In accordance with the above arguments, and in agreement with Fig. 7 (c), this quantity decreases with K_\perp . For the dotted line, the time variance was multiplied by β_K^2 . For the light pions, β_K^2 is close to unity already for moderate $K_\perp \sim 300$ MeV and the difference between these two curves rapidly vanishes with increasing K_\perp . For the long-dashed line the term $-2\beta_K \langle \tilde{x}\tilde{t} \rangle$ was added. Obviously, the $x - t$ -correlation of the emission function is negative and about 50% of the value of $\beta_K^2 \langle \tilde{t}^2 \rangle$. The dash-dotted line is the full result for \hat{R}_{out}^2 . As one notices, the variance in x -direction is only a minor correction to the other two terms. It is astonishing how well the approximate relations (16,17) reflect the qualitative *and* quantitative behaviour of the inverse widths of the correlation functions, although the shape of the emission function is not Gaussian. (Note that all variances appearing in eqs. (16,17) have been multiplied with a factor 1.44, to account for the difference in the definition of inverse widths and radii, as discussed at the end of Section 3.)

In Figs. 7 (d,f) we show the corresponding results for kaons. One observes that the emission function in the case $K_\perp = 300$ MeV is now somewhat narrower in time direction than in the pionic case. The reason is the larger kaon mass, or equivalently, the smaller kaon pair velocity which suppresses emission of such pairs from regions of the hypersurface with high flow velocity, i.e., at early times, cf. Fig. 7 (b). (Remember that the emission function is large in regions where pair and flow velocity are equal.) This effect leads to considerably smaller values for R_{out} and, as already discussed in the context of Figs. 4 and 5, $R_{\text{out}}/R_{\text{side}}$.

For larger K_\perp , however, the size of the region in time from which kaon pairs are predominantly emitted does not decrease very much, as one confirms via the time variance (dashed line in Fig. 7 (f)). This at first sight astonishing result is due to the fact that the flow velocity remains large up to very late times, cf. Fig. 7 (b), such that kaon pairs with high velocity are not only emitted at early times (where the flow velocity is high anyway), but also up to late times before the origin cools below $T = 0.7T_c$. The strong increase in the kaon pair velocity with K_\perp leads then to a corresponding *increase* in R_{out} and \hat{R}_{out} , cf. Fig. 7 (f). Note that due to the larger kaon mass, the difference between dashed and dotted curves is much bigger than for the pion case.

In Fig. 8 we present the corresponding results for the case $\Delta T = 0$ which serves to explain the behaviour observed in Fig. 6. In this case, the outward radii increase with K_{\perp} *both* for kaons *and* pions. The reason is that the emission functions, besides the shift of the maximum to earlier times, do not exhibit a decrease of the emission probability at late times, resulting in an overall *increase* in the duration of particle emission and, correspondingly, in the outward radii. From the above it is clear that due to the larger kaon mass, the increase of the outward radius with K_{\perp} is much stronger for kaons than for pions.

The reason for the increase in the width of the emission function is the behaviour of the flow velocity, Fig. 8 (b). Even up to times where the freeze-out reaches the origin, β stays comparatively large, enhancing the emission probability for particle pairs with high velocity. The physical reason for this high transverse velocity is a rarefaction shock wave (cf. Fig. 9 (a) in [10]), which travels inwards and expels matter with a constant flow velocity, a fact that is confirmed by the plateau observed in Fig. 8 (b) for times between 3 and 6 R_0 . Note again the excellent agreement between approximate radii, $\hat{R}_{\text{out,side}}$, and the inverse widths of the correlation functions, $R_{\text{out,side}}$, in Figs. 8 (e,f), although the emission functions are not even remotely resembling Gaussian distributions. In fact, for (16,17) to be good approximations of the inverse widths it is sufficient that the *correlation functions* resemble Gaussians, rather than the emission functions themselves. In most (realistic) situations, this happens to be the case ¹.

We finally mention that the high flow velocity in the cases of interest ensures that the negative contributions to the spectra and the correlation functions are negligible, as indicated in Subsection 2.3. Quantitatively, they are smaller than 1% (of the total particle number crossing the freeze-out hypersurface) for the smallest transverse momenta considered, $K_{\perp} \sim 100$ MeV. For larger transverse momenta, they are even smaller.

4 Summary and Conclusions

In this work we have investigated the time–delay effect of the QCD transition on two–pion and two–kaon correlations in ultrarelativistic heavy-ion collisions in the framework of ideal hydrodynamics with transverse cylindrical and boost-invariant longitudinal symmetry. Our study is an extension of the work in [10], where this time–delay signal, i.e., an enhanced ratio $R_{\text{out}}/R_{\text{side}}$, was investigated for pion interferometry with fixed average transverse pair momentum $K_{\perp} = 300$ MeV. Our main interest in the present work was the transverse momentum dependence of the proposed signal, and the question whether it can be also seen in two–kaon interferometry. Kaon interferometry seems preferable for two reasons. First, effects of resonance decays are small (only the shorter-lived K^* resonances influence the final kaon spectra, at most a (small) 10%–effect at temperatures corresponding to freeze-out [13]). For pion interferometry, however, the decay of long-lived resonances plays an important role and virtually increases the (average) source size and lifetime of the system [34]. This results in considerable modifications of the inverse width of the two–particle correlation functions of pions [13, 31, 35]. Second, neutral kaon correlation functions would not be influenced by

¹We thank U. Heinz for pointing this out.

final state Coulomb interactions at small relative momenta (where the correlation signal is large).

We presented a systematic study of the inverse widths R_{out} , R_{side} , and their ratio for two-pion and two-kaon correlation functions at midrapidity, as a function of the initial energy density ϵ_0 , the average transverse momentum of the particle pair K_{\perp} , and for different equations of state. Studying the emission functions and their variances for selected cases, we explained in detail the momentum dependence of the inverse width in out-direction. We confirmed that the prolongation of the lifetime of the system due to the QCD transition is observable in an enhanced ratio $R_{\text{out}}/R_{\text{side}}$ for kaons as well as for pions. The proposed signal is maximized for initial energy densities expected to be reached in central Au+Au-collisions at the RHIC collider, $\epsilon_0 \sim 10 - 20 \text{ GeV fm}^{-3}$ (for realistic [15] values of the initial thermalization time scale, $\tau_0 \sim 0.5 \text{ fm}$), and for pairs with high average transverse momentum, $K_{\perp} \sim 1 \text{ GeV}$. This opens the interesting possibility to observe the time-delay signal of the QCD transition with kaon interferometry in the STAR and PHENIX experiments at RHIC.

Acknowledgements

We would like to thank M. Gyulassy, T. Hallman, U. Heinz, B. Schlei, R. Pisarski, and W. Zajc for stimulating discussions. D.H.R. thanks in particular U. Heinz for encouraging this study, for a critical reading of the manuscript, and for invaluable help in interpreting the results. Special thanks go to M. Gyulassy for his continued support and encouragement throughout this work. D.H.R. gratefully acknowledges the hospitality of the Institute for Theoretical Physics of the University Frankfurt. The work of D.H.R. has been supported by the Director, Office of Energy Research, Division of Nuclear Physics of the Office of High Energy and Nuclear Physics of the U.S. Department of Energy under contract nos. DE-FG-02-93ER-40764 and DE-FG02-96ER40945.

Appendix

In this appendix we collect the explicit expressions necessary to evaluate the variances of the emission function $S(x, K)$ appearing in eqs. (16,17). We start with noting that

$$\begin{aligned}\langle \tilde{x}^2 \rangle &= \langle x^2 \rangle - \langle x \rangle^2, \\ \langle \tilde{t}^2 \rangle &= \langle t^2 \rangle - \langle t \rangle^2, \\ \langle \tilde{x}\tilde{t} \rangle &= \langle xt \rangle - \langle x \rangle \langle t \rangle, \\ \langle \tilde{y}^2 \rangle &= \langle y^2 \rangle - \langle y \rangle^2,\end{aligned}\tag{18}$$

while due to the δ -function in eq. (14), all space-time variables are taken along the freeze-out hypersurface Σ , given by the 4-vector

$$\Sigma^\mu = (\tau_f(\zeta) \cosh \eta, r_f(\zeta) \cos \phi, r_f(\zeta) \sin \phi, \tau_f(\zeta) \sinh \eta), \tag{19}$$

with $r_f(\zeta)$, $\tau_f(\zeta) \equiv t_f(\zeta, \eta = 0)$, given by the isotherms in Figs. 7, 8 (a). Here we adhered to the notation of Ref. [10], i.e., the hypersurface Σ is parametrized by the three variables ζ , η , and ϕ , where ζ runs from 0 to 1 along the hypersurface in the $(t-r)$ -plane at $z=0$, η from $-\infty$ to ∞ along the hypersurface in the $(t-z)$ -plane (η is identical to the space-time rapidity $\text{Artanh}[z/t]$) and ϕ from 0 to 2π in the transverse $(x-y)$ -plane. Due to the transverse cylindrical and boost-invariant longitudinal symmetry of the problem, the parametrization of the hypersurface in terms of ϕ and η is trivial. Note that for $z = \eta = 0$, $\tau \equiv \sqrt{t^2 - z^2} \equiv t$.

Using the definition of the average $\langle \cdot \rangle$ in eq. (13), we find after employing (cf. eq. (B.3) of [10])

$$d\Sigma \cdot K = \left(-E_K \cosh \eta \frac{dr_f}{d\zeta} + K_\perp \cos \phi \frac{d\tau_f}{d\zeta} \right) r_f(\zeta) \tau_f(\zeta) d\zeta d\eta d\phi, \tag{20}$$

where we used $K^0 \simeq E_K$, $\mathbf{K} = (K_\perp, 0, 0)$, and (cf. eq. (B.4) of [10])

$$K \cdot u = E_K \cosh \eta \cosh \eta_r - K_\perp \sinh \eta_r \cos \phi, \tag{21}$$

where $\eta_r \equiv \text{Artanh} \beta$ (β is the radial component of the transverse velocity at $z=0$), and after integrating over η , ϕ the final result:

$$\langle x \rangle = \mathcal{N}^{-1} \int_0^1 d\zeta r_f^2 \tau_f \left\{ -E_K \frac{dr_f}{d\zeta} K_1(a) I_1(b) + K_\perp \frac{d\tau_f}{d\zeta} K_0(a) \left[I_0(b) - \frac{I_1(b)}{b} \right] \right\}, \tag{22}$$

$$\langle y \rangle = 0, \tag{23}$$

$$\langle t \rangle = \mathcal{N}^{-1} \int_0^1 d\zeta r_f \tau_f^2 \left\{ -E_K \frac{dr_f}{d\zeta} \left[K_0(a) + \frac{K_1(a)}{a} \right] I_0(b) + K_\perp \frac{d\tau_f}{d\zeta} K_1(a) I_1(b) \right\}, \tag{24}$$

$$\begin{aligned}\langle x^2 \rangle &= \mathcal{N}^{-1} \int_0^1 d\zeta r_f^3 \tau_f \left\{ -E_K \frac{dr_f}{d\zeta} K_1(a) \left[I_0(b) - \frac{I_1(b)}{b} \right] \right. \\ &\quad \left. + K_\perp \frac{d\tau_f}{d\zeta} K_0(a) \left[-\frac{I_0(b)}{b} + \left(1 + \frac{2}{b^2} \right) I_1(b) \right] \right\},\end{aligned}\tag{25}$$

$$\begin{aligned} \langle y^2 \rangle = \mathcal{N}^{-1} \int_0^1 d\zeta r_f^3 \tau_f^3 \left\{ -E_K \frac{dr_f}{d\zeta} K_1(a) \frac{I_1(b)}{b} \right. \\ \left. + K_\perp \frac{d\tau_f}{d\zeta} K_0(a) \left[\frac{I_0(b)}{b} - \frac{2 I_1(b)}{b^2} \right] \right\} , \end{aligned} \quad (26)$$

$$\begin{aligned} \langle t^2 \rangle = \mathcal{N}^{-1} \int_0^1 d\zeta r_f \tau_f^3 \left\{ -E_K \frac{dr_f}{d\zeta} \left[\frac{K_0(a)}{a} + \left(1 + \frac{2}{a^2} \right) K_1(a) \right] I_0(b) \right. \\ \left. + K_\perp \frac{d\tau_f}{d\zeta} \left[K_0(a) + \frac{K_1(a)}{a} \right] I_1(b) \right\} , \end{aligned} \quad (27)$$

$$\begin{aligned} \langle xt \rangle = \mathcal{N}^{-1} \int_0^1 d\zeta r_f^2 \tau_f^2 \left\{ -E_K \frac{dr_f}{d\zeta} \left[K_0(a) + \frac{K_1(a)}{a} \right] I_1(b) \right. \\ \left. + K_\perp \frac{d\tau_f}{d\zeta} K_1(a) \left[I_0(b) - \frac{I_1(b)}{b} \right] \right\} , \end{aligned} \quad (28)$$

$$\mathcal{N} = \int_0^1 d\zeta r_f \tau_f \left\{ -E_K \frac{dr_f}{d\zeta} K_1(a) I_0(b) + K_\perp \frac{d\tau_f}{d\zeta} K_0(a) I_1(b) \right\} , \quad (29)$$

where $a \equiv E_K \cosh \eta_r / T$, $b \equiv K_\perp \sinh \eta_r / T$.

References

- [1] F. Karsch, Nucl. Phys. B (Proc. Suppl.) 34 (1994) 63, Phys. Rev. D 49 (1994) 3791, E. Laermann, Nucl. Phys. A 610 (1996) 1c.
- [2] B. Müller, Rep. Prog. Phys. 58 (1995) 611.
- [3] J.W. Harris and B. Müller, Annu. Rev. Nucl. Part. Sci. 46 (1996) 71.
- [4] R.B. Clare and D.D. Strottman, Phys. Rep. 141 (1986) 177.
- [5] C.M. Hung and E.V. Shuryak, Phys. Rev. Lett. 75 (1995) 4003.
- [6] D.H. Rischke, S. Bernard, J.A. Maruhn, Nucl. Phys. A 595 (1995) 346.
- [7] D.H. Rischke and M. Gyulassy, Nucl. Phys. A 597 (1996) 701.
- [8] L.V. Bravina, N.S. Amelin, L.P. Csernai, P. Levai, D. Strottman, Nucl. Phys. A 566 (1994) 461c.
- [9] D.H. Rischke, Y. Pürsün, J.A. Maruhn, H. Stöcker, W. Greiner, Heavy Ion Phys. 1 (1995) 309.
- [10] D.H. Rischke and M. Gyulassy, Nucl. Phys. A 608 (1996) 479.
- [11] S. Pratt, Phys. Rev. C 49 (1994) 2722, Phys. Rev. D 33 (1986) 1314.
- [12] G. Bertsch, M. Gong, M. Tohyama, Phys. Rev. C 37 (1988) 1896, G. Bertsch, Nucl. Phys. A 498 (1989) 173c.
- [13] J. Bolz, U. Ornik, M. Plümer, B.R. Schlei, R.M. Weiner, Phys. Rev. D 47 (1993) 3860, B. Schlei, U. Ornik, M. Plümer, D. Strottman, R.M. Weiner, Phys. Lett. B 376 (1996) 212.
- [14] U.A. Wiedemann, P. Scotto, U. Heinz, Phys. Rev. C 53 (1996) 918, U. Heinz, lectures given at the NATO ASI on “Correlations and Clustering Phenomena in Subatomic Physics”, Dronten, Netherlands, August 4 – 18, 1996, LANL preprint server nucl-th/9609029.
- [15] E. Shuryak, Phys. Rev. Lett. 68 (1992) 3270, K.J. Eskola and M. Gyulassy, Phys. Rev. C 47 (1993) 2329.
- [16] L.D. Landau and E.M. Lifshitz, “Fluid mechanics” (Pergamon, New York, 1959).
- [17] J.D. Bjorken, Phys. Rev. D 27 (1983) 140, G. Baym, B.L. Friman, J.P. Blaizot, M. Soyeur, W. Czyż, Nucl. Phys. A 407 (1983) 541.
- [18] M. Gyulassy, D.H. Rischke, B. Zhang, Nucl. Phys. A 613 (1997) 397.

- [19] G.A. Sod, *J. Fluid Mech.* 83 (1977) 785.
- [20] V. Schneider et al., *J. Comput. Phys.* 105 (1993) 92.
- [21] D.H. Rischke, Y. Pürsün, J.A. Maruhn, *Nucl. Phys. A* 595 (1995) 383.
- [22] J.P. Blaizot and J.Y. Ollitrault, *Phys. Rev. D* 36 (1987) 916.
- [23] A. Chodos, R.L. Jaffe, K. Johnson, C.B. Thorn, V.F. Weisskopf, *Phys. Rev. D* 9 (1974) 3471.
- [24] C. Greiner and C. Spieles, private communication (preprint in preparation).
- [25] K.A. Bugaev, *Nucl. Phys. A* 606 (1996) 559.
- [26] J.J. Neumann, B. Lavrenchuk, G. Fai, LANL preprint server nucl-th/9612020.
- [27] F. Cooper and G. Frye, *Phys. Rev. D* 10 (1974) 186,
F. Cooper, G. Frye, E. Schonberg, *Phys. Rev. D* 11 (1975) 192.
- [28] S. Bernard, J.A. Maruhn, W. Greiner, D.H. Rischke, *Nucl. Phys. A* 605 (1996) 566.
- [29] Yu.M. Sinyukov, *Z. Phys. C* 43 (1989) 401.
- [30] Yu.M. Sinyukov, *Nucl. Phys. A* 498 (1989) 151c.
- [31] B.R. Schlei, U. Ornik, M. Plümer, R.M. Weiner, *Phys. Lett. B* 293 (1992) 275.
- [32] F. Yano and S. Koonin, *Phys. Lett. B* 78 (1978) 556,
M.I. Podgoretskii, *Sov. J. Nucl. Phys.* 37 (1983) 272,
S. Chapman, J.R. Nix, U. Heinz, *Phys. Rev. C* 52 (1995) 2694.
- [33] J. Alam, D.K. Srivastava, B. Sinha, D.N. Basu, *Phys. Rev. D* 48 (1993) 1117.
- [34] S.S. Padula and M. Gyulassy, *Nucl. Phys. A* 544 (1992) 537c.
- [35] B.R. Schlei, Los Alamos preprint LA-UR-96-1614, LANL preprint server nucl-th/9605016,
U.A. Wiedemann and U. Heinz, LANL preprint server nucl-th/9611031.

Figure Captions:

Fig. 1: (a) The entropy density divided by T^3 (in units of s_c/T_c^3), (b) the energy density divided by T^4 (in units of $T_c s_c/T_c^4$) as functions of temperature (in units of T_c), (c) the pressure (in units of $T_c s_c$), (d) the square of the velocity of sound as functions of energy density (in units of $T_c s_c$). The solid lines correspond to $\Delta T = 0$, the dotted curves to $\Delta T = 0.1 T_c$. Quantities for the ideal gas EoS (with d_H degrees of freedom) are represented by dashed lines. The ratio of degrees of freedom in the QGP to those in the hadronic phase is $d_Q/d_H = 37/3$. The critical enthalpy density is $T_c s_c \simeq 0.75 \text{ GeV fm}^{-3}$ for the case $d_Q = 37$, $d_H = 3$.

Fig. 2: $R_{\text{out}}/R_{\text{side}}$ as a function of the initial energy density ϵ_0 for the Bjorken cylinder expansion ($\tau_0 = 0.1 R_0$) with a first order phase transition ($\Delta T = 0$). Thin lines correspond to pion pairs ($m_\pi = 138 \text{ MeV}$), thick lines to kaons ($m_K = 497 \text{ MeV}$). The pairs are at midrapidity and have average transverse momentum $K_\perp = 300 \text{ MeV}$. The results are shown for freeze-out temperatures $T_f = 0.7 T_c$ (full lines), $T_f = 0.9 T_c$ (dotted lines), and $T_f = T_c$ (dashed lines).

Fig. 3: $R_{\text{out}}/R_{\text{side}}$ for kaons as a function of the initial energy density ϵ_0 at $K_\perp = 700 \text{ MeV}$. The ideal gas case (thin lines) is compared to that of a first order phase transition (thick lines, $\Delta T = 0$). Curves correspond to different freeze-out temperatures as in Fig. 2.

Fig. 4: The dependence of $R_{\text{out}}/R_{\text{side}}$ on the average transverse momentum K_\perp of the particle pair, for fixed energy density $\epsilon_0 = 18.75 T_c s_c$. Thin lines correspond to pions, thick lines to kaons. Different curves correspond to different freeze-out temperatures, as in Fig. 2.

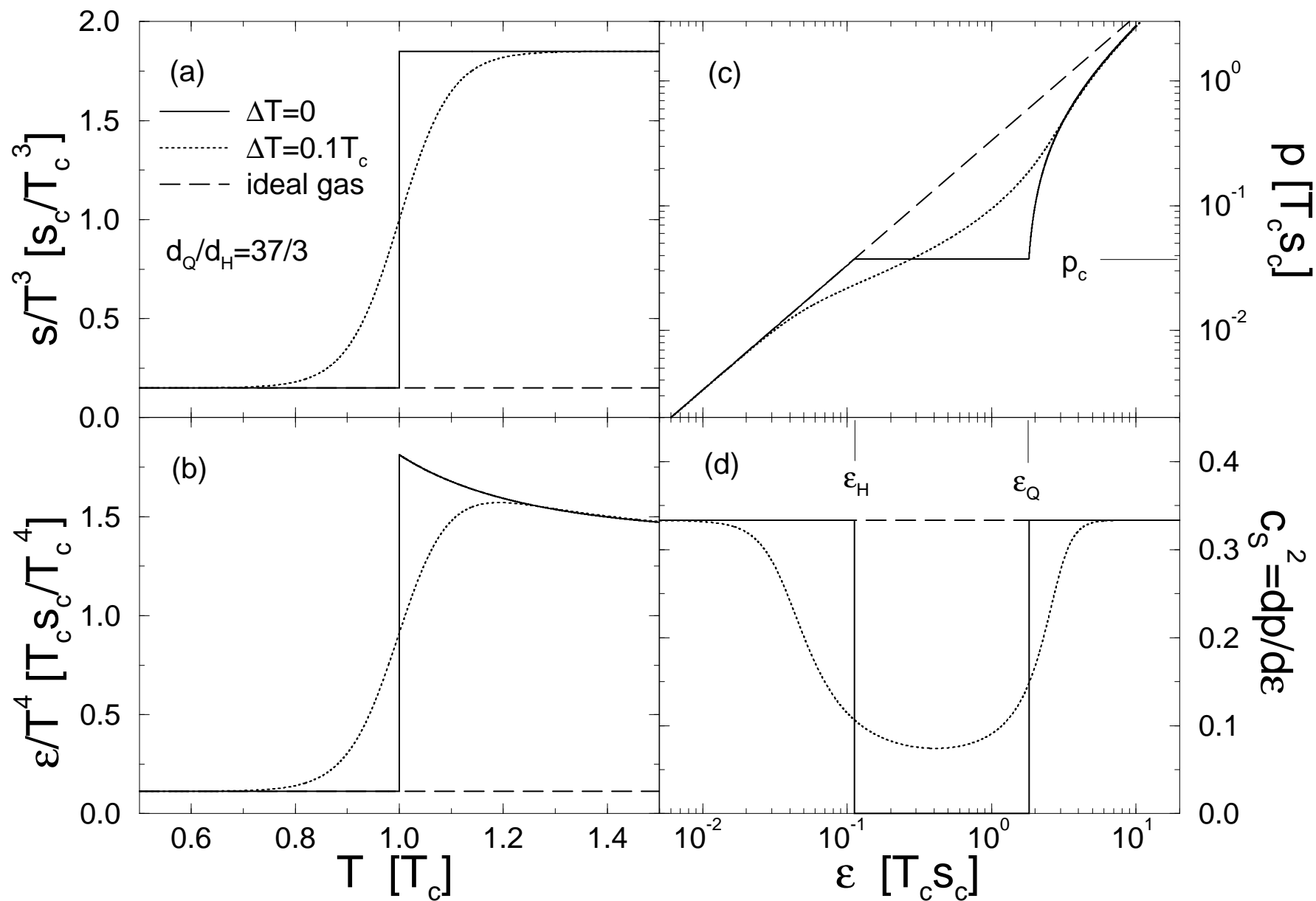
Fig. 5: (a) $R_{\text{out}}/R_{\text{side}}$ as a function of ϵ_0 and K_\perp for pions at midrapidity and freeze-out temperature $T_f = 0.7 T_c$, for the case of a first order phase transition ($\Delta T = 0$, full lines) versus the ideal gas case (dotted). (b) as in (a), but for $\Delta T = 0.1 T_c$. (c,d) as in (a,b), but for kaons.

Fig. 6: (a) Inverse width of the pion correlation function in out-direction R_{out} (in units of the initial transverse radius R_0) at midrapidity and for $\Delta T = 0$, as a function of ϵ_0 and K_\perp . (b) as in (a), but for R_{side} . (c,d) as in (a,b), but for kaons.

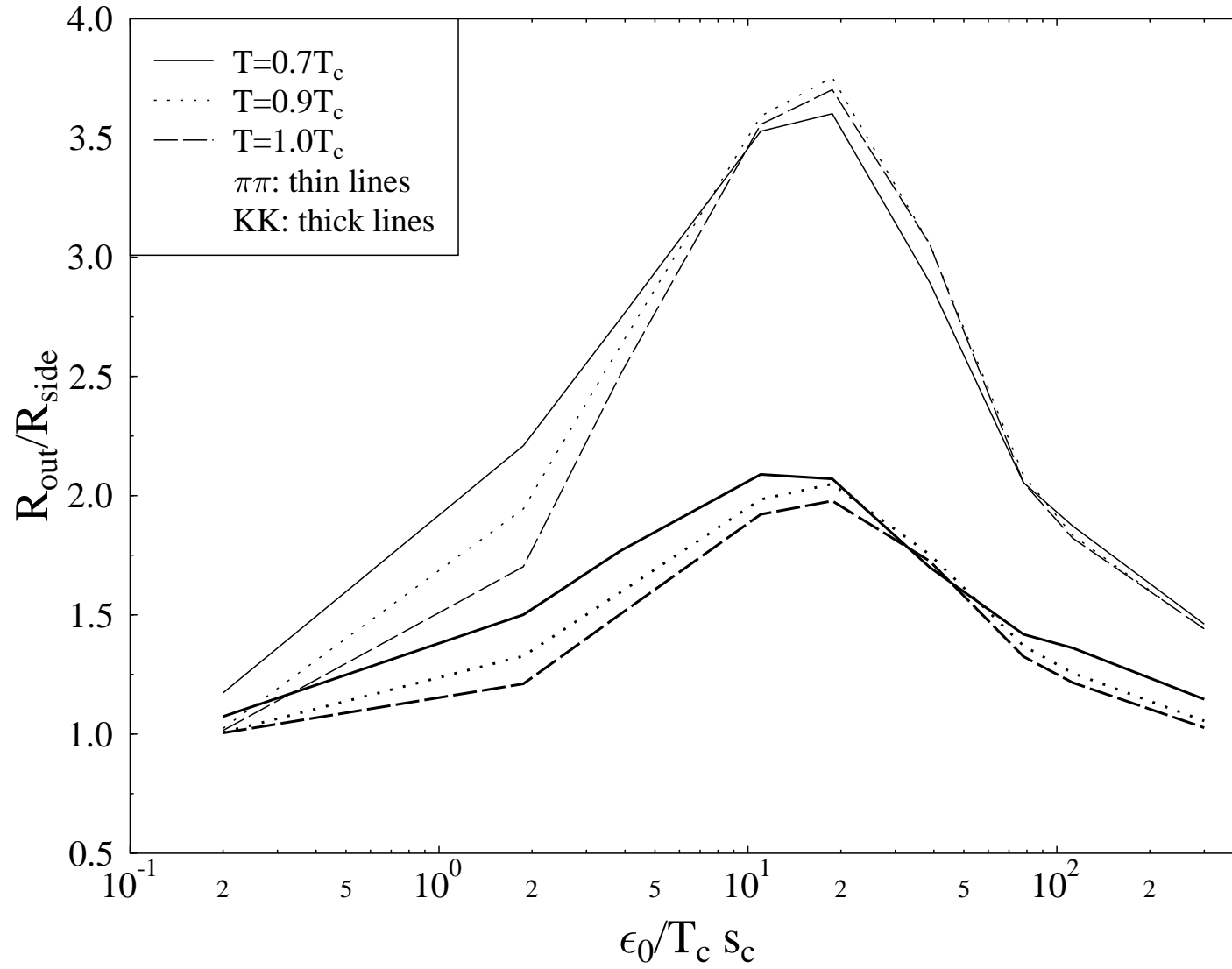
Fig. 7: (a) Isotherms in the $(t - r)$ -plane (at $z = 0$) for the hydrodynamic expansion of a Bjorken cylinder with $\epsilon_0 = 18.75 T_c s_c$, $\tau_0 = 0.1 R_0$, and for a smooth transition $\Delta T = 0.1 T_c$ in the EoS. Labels correspond to temperatures in units of T_c . The freeze-out isotherm ($T_f = 0.7 T_c$) is the thick line. (b) The flow velocity β as a function of time along the freeze-out isotherm of part (a). (c) The emission function for pions (in arbitrary units), integrated over η and ϕ (and smoothed over approximately 100 time steps of the hydrodynamical evolution), along the freeze-out isotherm of part (a), for $K_\perp = 300 \text{ MeV}$ (solid line), $K_\perp = 700 \text{ MeV}$ (dotted line), and $K_\perp = 1000 \text{ MeV}$ (long-dashed line). (d) as in (c), but for kaons. (e) R_{out}^2 and R_{side}^2 for pions as a function of K_\perp (solid lines), and the approximate

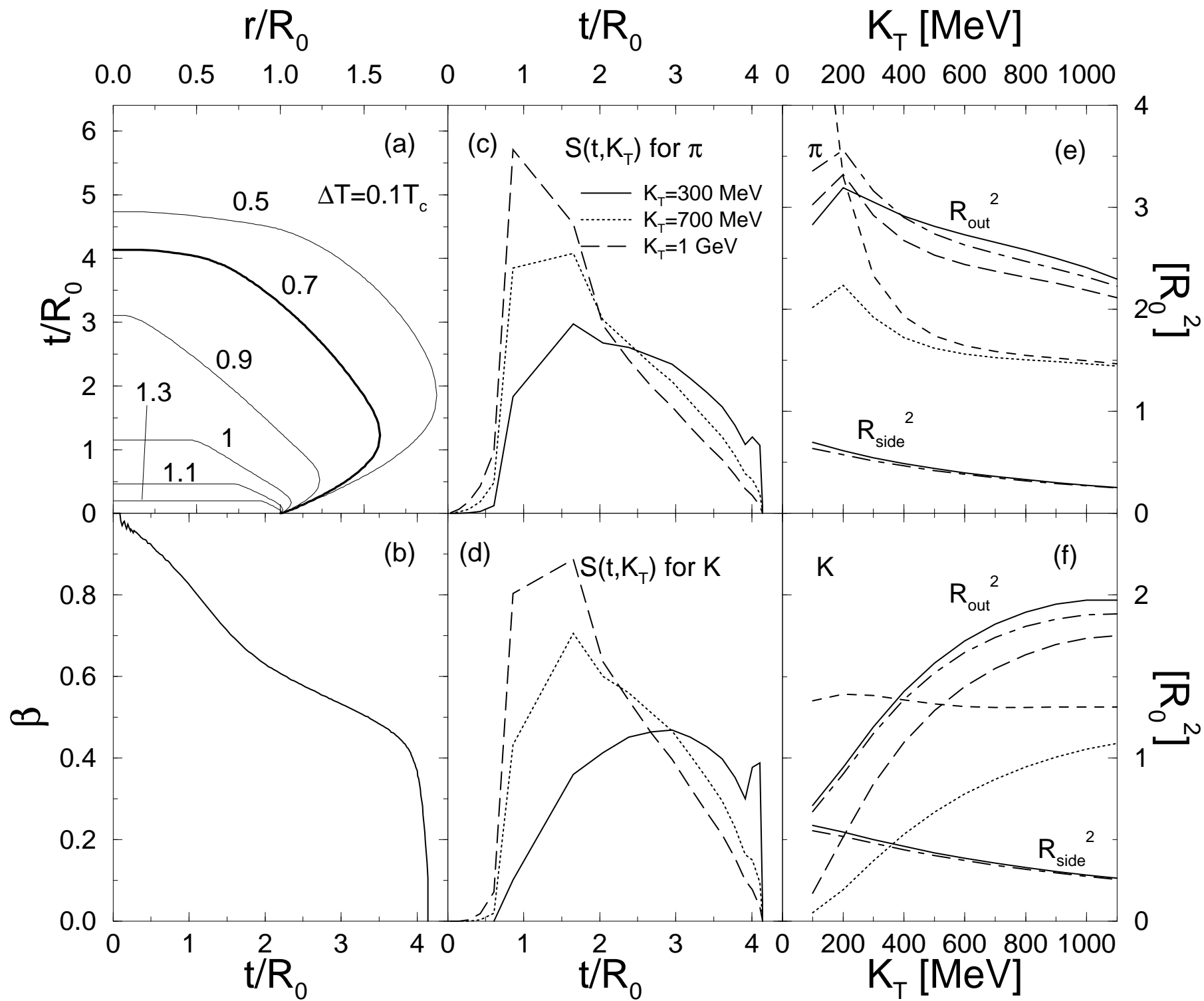
radii \hat{R}_{out}^2 and \hat{R}_{side}^2 (dash-dotted lines). The dashed line is the variance in time only, $\langle \tilde{t}^2 \rangle$, while for the dotted line, this quantity was multiplied with β_K^2 . For the long-dashed line, the $x - t$ -correlation $-2\beta_K \langle \tilde{x}\tilde{t} \rangle$ has been added. (f) as in (e), but for kaons.

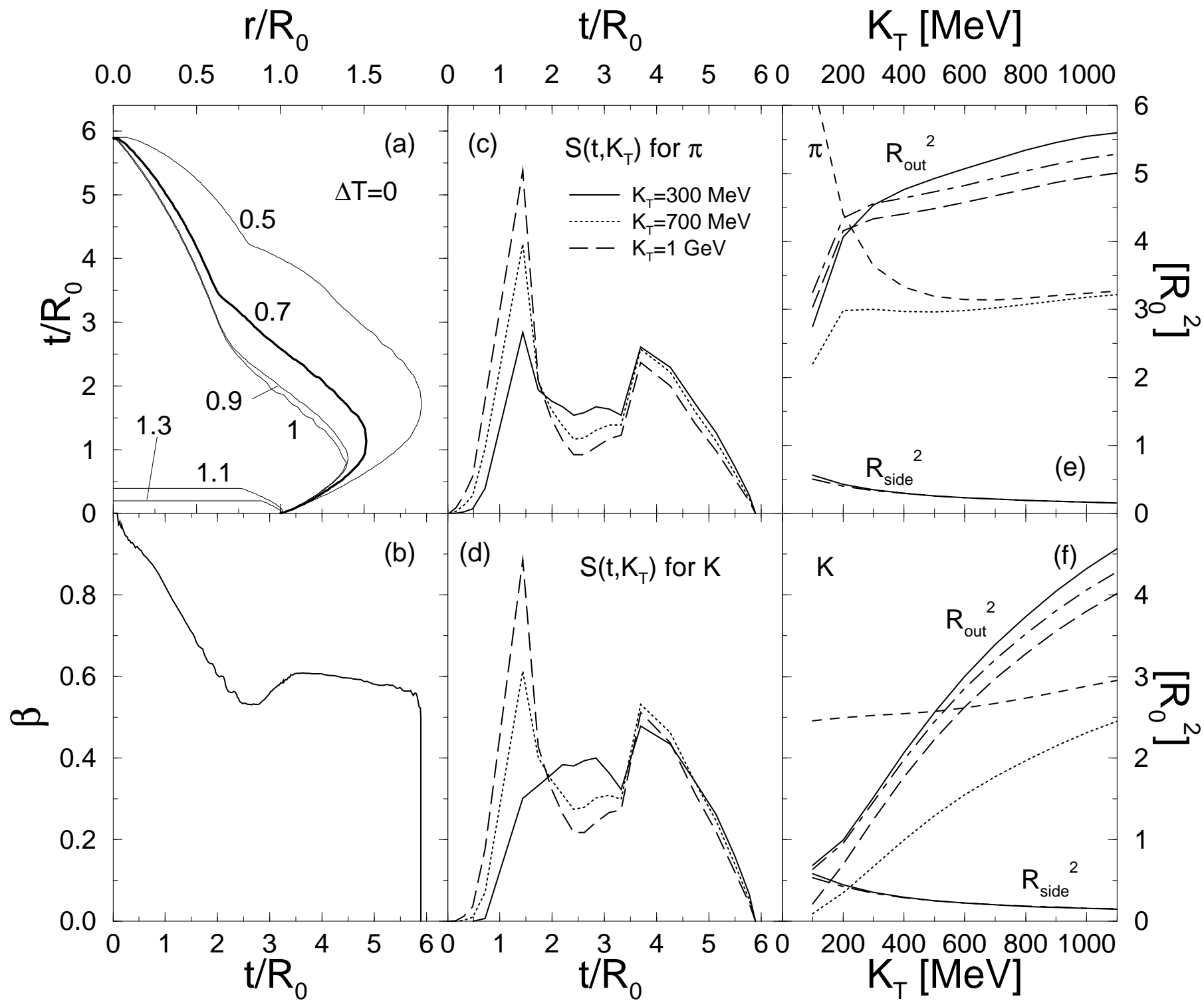
Fig. 8: As in Fig. 7, but for $\Delta T = 0$.



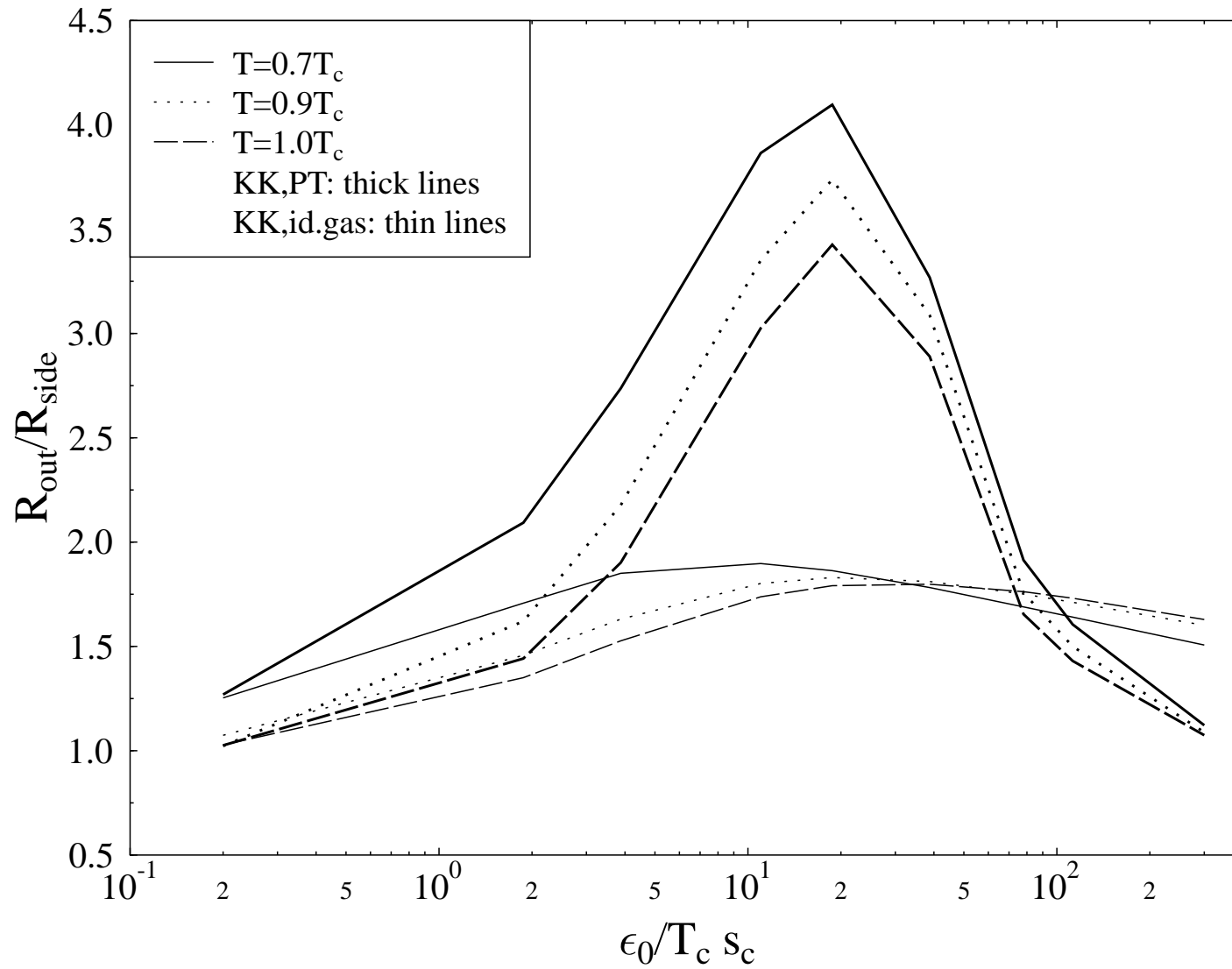
$K_{\perp}=300\text{MeV}, B_{j+\text{Cyl}}$







$K_{\perp}=700\text{MeV}, B_j+\text{Cyl}$



$\epsilon_0=18.75T_c s_c$, Bj+Cyl

